Biomacromolecules

Article

Cite This: Biomacromolecules 2019, 20, 1281−1287

pubs.acs.org/Biomac

Peptidic Monodisperse PEG "combs" with Fine-Tunable LCST and Multiple Imaging Modalities

Junfei Zhu,[†] Yan Xiao,[‡] Huaibin Zhang,[†] Yu Li,[†] Yaping Yuan,[§] Zhigang Yang,[†] Shizhen Chen,[§] Xing Zheng,[‡] Xin Zhou,[§] and Zhong-Xing Jiang*[,†]

[†]Hubei Province Engineering and Technology Research Center for Fluorinated Pharmaceuticals, School of Pharmaceutical Sciences, Wuhan University, Wuhan 430071, China

[‡]Institute of Pharmacy and Pharmacology, University of South China, Hengyang 421001, China

[§]State Key Laboratory for Magnetic Resonance and Atomic and Molecular Physics, National Center for Magnetic Resonance in Wuhan, Wuhan Institute of Physics and Mathematics, Chinese Academy of Sciences, Wuhan 430071, China

Supporting Information

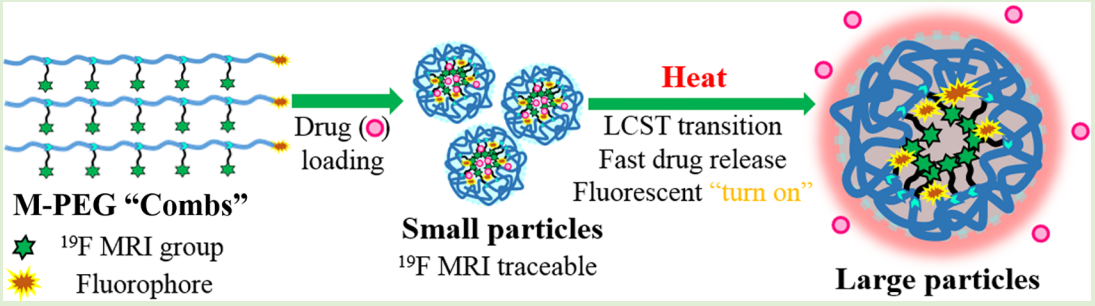

ABSTRACT: Thermosensitive and imaging-traceable materials with fine-tunable lower critical solution temperature (LCST) around body temperature are highly valuable in biomedicine. However, such materials are rare because it is challenging to fine-tune the LCST and incorporate suitable imaging modalities. Herein, peptidic monodisperse polyethylene glycol (M-PEG) "combs" with fine-tunable LCST, "hot spot" fluorine-19 magnetic resonance imaging (^{19}F MRI), thermoresponsive fluorescent imaging, and drug loading ability were developed through accurately programming their structures during solid phase peptide synthesis (SPPS). The easy availability, structural accuracy, biocompatibility, and versatility provide the M-PEG "combs" with promising prospects as thermoresponsive and imaging-traceable biomaterials for controlled drug delivery.

INTRODUCTION

In recent years, thermosensitive biomaterials have attracted considerable attention in drug delivery, tissue engineering, biosensing, and so on.[1−6] Taking drug delivery as an example, thermosensitive drug carriers, most of which are amphiphilic block copolymers, can release drugs at the pathogen sites in a highly controllable fashion through phase transitions triggered by pathogenic local hyperthermia or high intensity focused ultrasound.[7−11] When treating human diseases with a thermosensitive drug delivery system, a sharp and tunable LCST slightly above body temperature is crucial for achieving controlled drug release and high therapeutic efficacy. However, thermosensitive amphiphilic block copolymers with such a LCST are rare, and tuning the LCST of the existing thermosensitive amphiphilic block copolymers is challenging due to their structural complexity. In addition, few imaging modalities in existing thermosensitive amphiphilic block copolymers are available for monitoring the drug delivery and controlled release process. Therefore, it is of great importance to develop novel imaging-traceable and thermosensitive materials with sharp and fine-tunable LCSTs around body temperature.

Basically, the LCST of a material is mainly determined by its chemical structure. Thus, the more accurately the structure of a material is manipulated, the better its LCST is fine-tuned. Structurally, most thermosensitive materials in biomedicine are amphiphilic block copolymers.[12−16] Among the block copolymers, PEG block copolymers are the most used thermosensitive biomaterials due to their high biocompatibility.[17−19] However, it is very challenging to accurately manipulate the structure of a PEG block copolymer because of numerous components and multiple reaction centers in these polydisperse materials. Thus, the development of amphiphilic M-PEGs-based biomaterials with structural accuracy and diversity may lead to thermosensitive biomaterials of sharp and fine-tunable LCSTs.[20−24]

With the development of novel synthetic methods for M-PEGs,[25−28] M-PEGs and alternatives have been increasingly used biomedicine.[29−31] Now, some low molecular weight M-PEGs and derivatives are commercially available. Recently, M-

Received: November 25, 2018
Revised: January 17, 2019
Published: January 22, 2019

DOI: 10.1021/acs.biomac.8b01693
Biomacromolecules 2019, 20, 1281−1287

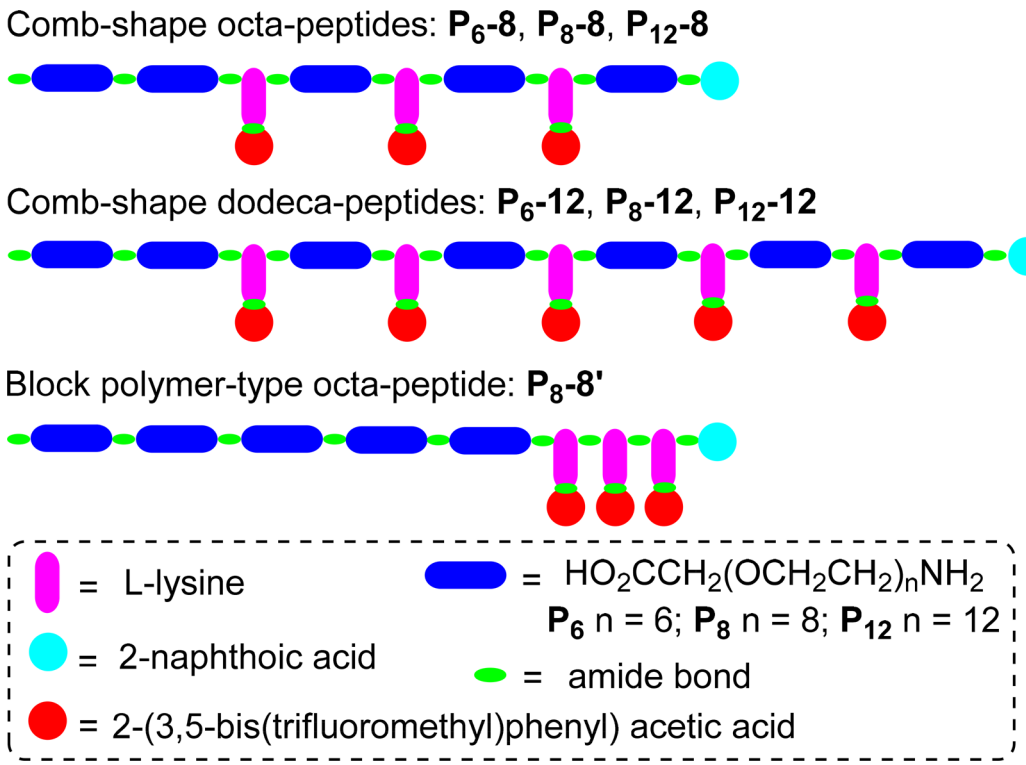

Figure 1. Designed thermosensitive peptidic M-PEG "combs".

PEGs modified drugs, peptides, and imaging agents were developed in this group.[32−35] It was found that the monodispersity of PEG is crucial for achieving optimal physicochemical and biological properties. Moreover, manipulating the size of M-PEGs has been proven as a convenient and efficient way to fine-tune the properties of M-PEG-based materials. Therefore, amphiphilic M-PEGs-based materials may avoid the issues of thermosensitive block copolymers and achieve sharp and fine-tunable LCSTs. Herein, we took the advantage of peptide chemistry and developed oligopeptide-based amphiphilic M-PEG "combs" with sharp and fine-tunable LCSTs as image-traceable and thermosensitive biomaterials (Figure 1). The versatile SPPS provided a highly programmable strategy to accurately manipulate the chemical structure and incorporate multifunctions, such as imaging modality, targeting molecule, drug loading, and so on. In the M-PEG "combs", M-PEG-containing ω-amino acids were employed as hydrophilicity backbones and biocompatibility enhancers. 2-(3,5-Bis(trifluoromethyl)-phenyl) acetic acid modified L-lysines were evenly inserted into the peptidic M-PEG backbone to induce self-assembly through hydrophobic interactions. For the convenience of purification in peptide synthesis and imaging in downstream applications, 2-naphthoic acid was employed as a UV and fluorescent tag to block *N*-terminals of the M-PEG "combs". Because comb-shape polymers usually exhibit superior physicochemical properties compared to their block copolymer counterparts,[36−40] oligopeptides of such M-PEG "combs" may achieve the desired physicochemical properties of high molecular weight PEG block copolymers (usually >10000 Da). Because they have much lower molecular weights than PEG block copolymers, it is much easier to synthesize and accurately manipulate the structure of the M-PEG "combs". Finally, a unified strong ^{19}F NMR signal from multiple pseudosymmetrical fluorines in the peptide would facilitate sensitive "hot-spot" ^{19}F MRI tracking of the M-PEG "combs". Based on these concerns, comb-shape M-PEG octa-peptides (**P_6-8**, **P_8-8**, and **P_{12}-8**) and dodeca-peptides (**P_6-12**, **P_8-12**, and **P_{12}-12**), together with a block copolymer-type M-PEG control peptide **P_8-8′** were designed (Figure S1).

EXPERIMENTAL SECTION

Synthesis and Purification of Peptidic M-PEG "Combs". The peptidic M-PEG "combs" were manually synthesized through the Fmoc-strategy in a sintered glass reaction funnel fitted with a three-way stopcock on Rink amide-AM resin. Coupling reactions were performed in DMF for 2 h with 2.5 equiv of Fmoc-protected amino acid, which was activated in situ with either 2.5 equiv of HATU and 5.0 equiv of DIPEA or 2.5 equiv of HOBt, 2.5 equiv of TBTU, and 5.0 equiv of DIPEA in DMF. Double coupling reactions were carried out on each residue. The coupling efficiency was assessed by TNBS test (1% picrylsulfonic acid in DMF and 10% *N*,*N*-diisopropylethylamine in DMF) for 5 min. Deprotection reactions were performed by treating the resin 5 min with a cocktail of either piperidine/DMF (2:8) or piperidine/DBU/DMF (2:2:96) for several times. The target peptide (peptidic M-PEG "comb") was released from the resin with a solution of TFA/TES/DCM (20:1:20). The crude peptide was purified with preparative reverse phase HPLC (UV detection at 254 nm, RP C18 column (10 μm; 30 mm × 250 mm), gradient elution from 60% methanol in water to 100% methanol over 60 min, flow rate 10 mL/min). The purity of the peptidic M-PEG "combs" was evaluated on reverse phase HPLC.

Preparation of DOX- or BODIPY-Loaded Nanoemulsions. Solvent evaporation method was used for DOX loaded nanoemulsion formulation. DOX·HCl (2 mg) and TEA (3 equiv) in 2 mL of DCM was stirred at rt for 2 h. The resulting mixture was evaporated under vacuum and the residue was suspended in 0.2 mL DCM to which **P_{12}-12** (10 mg in 0.2 mL of DCM) was added. The resulting mixture was injected into 5 mL of deionized water under sonicating over 30 min. The organic solvent was evaporated under reduced pressure at room temperature. The red solution was filtered twice through a 0.45 μm

DOI: 10.1021/acs.biomac.8b01693
Biomacromolecules 2019, 20, 1281−1287

polycarbonate membrane. The amount of DOX in the nanoemulsion was measured by HPLC. Film dispersion method was employed for BODIPY-loaded nanoemulsion formulation. A mixture of $\mathbf{P_{12}}$-**12**/BODIPY (30 mg/1 mg) in 2 mL of DCM was evaporated on a vacuum rotavapor to form a dry film on the wall of the flask. Deionized water (2.0 mL) was added to the flask and the flask was sonicated at 60 °C for 1 h, then sequentially filtered twice through 0.45 and 0.22 μm polycarbonate membranes. The amount of BODIPY loaded in the nanoemulsion was measured by HPLC.

Cellular Uptake. After seeding HepG2 cells in confocal dishes and culturing for 24 h, free DOX (5 μg/mL) or $\mathbf{P_{12}}$-**12** + DOX nanoemulsion (equivalent DOX concentration: 5 μg/mL) was added and the cells were incubated at 37 °C for 0.5 or 2 h, respectively. Then, the supernatant was carefully removed and the cells were washed with PBS buffer. The cells were fixed with 4% formaldehyde for 20 min at room temperature and washed three times with PBS. After staining with 4,6-diamidino-2-phenylindole (DAPI) for 5 min, the cells were imaged with confocal laser scanning microscopy (Leica-LCS-SP8-STED).

In Vitro ^{19}F MRI Experiments. All magnetic resonance imaging (MRI) experiments were performed on a 400 MHz Bruker BioSpec MRI system. The temperature of the magnet room was maintained at 25 °C during the entire MRI experiment. $\mathbf{P_{12}}$-**12** solutions (4, 2.7, 2, 1.3, 0.67, and 0.33 mM) were prepared by sequential dilution with deionized water. The ^{19}F in vitro images were acquired using a gradient-echo (GRE) pulse sequence, method = RARE, matrix size = 32 × 32, SI = 37 mm, FOV = 3.7 cm, TR = 4000 ms, TE = 7.0 ms, scan time = 32 s, B = 9.4 T.

In Vivo Fluorescence Imaging. A total of 250 μL of BODIPY-loaded micelles (corresponding to 0.6 μmol/kg) was intravenously injected into the HepG2 tumor-bearing mice. The fluorescent scans were recorded on Bruker Xtreme BI (U.S.A.). Fluorescence imaging was performed using a 690 nm excitation and a 750 nm emission filter.

RESULTS AND DISCUSSION

Synthesis and Characterization of Peptidic M-PEG "combs". The peptidic M-PEG "comb" synthesis started with amino acids construction. Through a macrocyclic sulfate-based strategy,[28] the ω-amino acids with 6, 8, and 12 ethylene glycol units were conveniently prepared in Fmoc-protected forms on 10 g scales, respectively. 2-(3,5-Bis(trifluoromethyl)-phenyl) acetic acid modified L-lysine was prepared from a commercially available L-lysine derivative. Then, the designed peptides were prepared through Fmoc-strategy on solid phase. After HPLC purification, the peptidic M-PEG "combs" were obtained on multihundred milligram scales with high purity and full characterization (see Supporting Information).

With the peptidic M-PEG "combs" in hand, their thermosensitive property was then studied with the aid of turbidity curves. As a result of their peculiar mode of interactions, LCSTs were observed from all the M-PEG "combs". But, no LCST was observed in the range of 10−100 °C for M-PEGs block copolymer $\mathbf{P_8}$-**8′**. As thermosensitive M-PEG "combs" $\mathbf{P_8}$-**8** and nonthermosensitive M-PEGs block copolymer $\mathbf{P_8}$-**8′** had the same molecular weight and amino acid components, it is the "combs"-shape allocation of hydrophobic L-lysine derivatives resulted in the thermosensitive property of these amphiphilic M-PEG "combs". Comparing to polydisperse PEGs-containing block polymers,[41] all the M-PEG "combs" gave very sharp LCSTs due to their structural accuracy. Moreover, the LCSTs of the M-PEG "combs" can be fine-tuned by structural modification in two ways: (1) Increasing the length of M-PEGs fragments in the M-PEG "combs" elevated the LCSTs (Figure 2a, serial 1: $\mathbf{P_6}$-**12** (10 °C), $\mathbf{P_8}$-**12** (26 °C), $\mathbf{P_{12}}$-**12** (43 °C); serial 2: $\mathbf{P_6}$-**8** (31 °C),

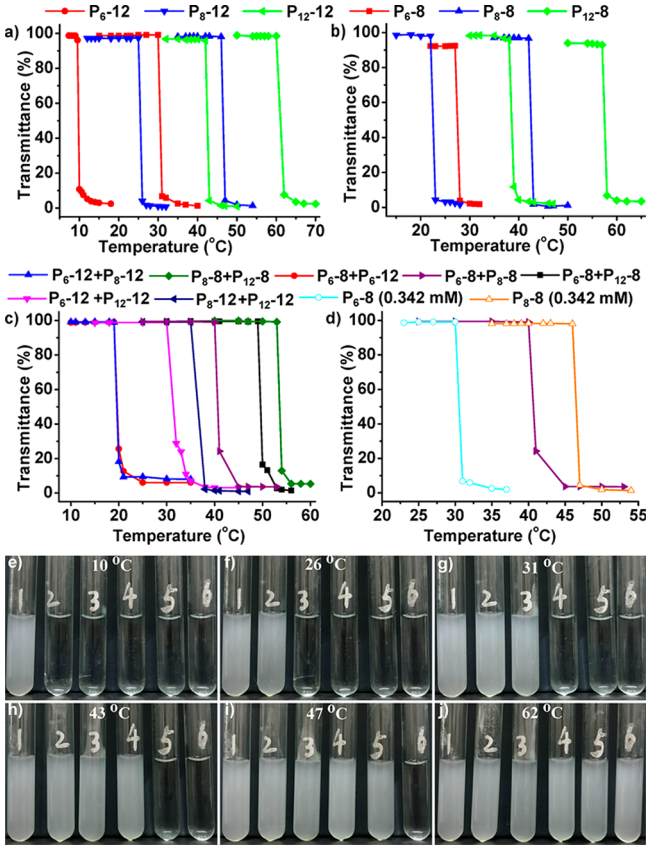

Figure 2. Turbidity curves of M-PEG peptides (a: 0.342 mM, b: 3.42 mM, c: mixtures of 0.171 mM each peptide; d: $\mathbf{P_6}$-**8**, $\mathbf{P_8}$-**8**, and their mixture) and photos of M-PEG peptides at 10−62 °C (tubes 1−6 contain 0.342 mM of $\mathbf{P_6}$-**12**, $\mathbf{P_8}$-**12**, $\mathbf{P_6}$-**8**, $\mathbf{P_{12}}$-**12**, $\mathbf{P_8}$-**8**, and $\mathbf{P_{12}}$-**8**, respectively).

$\mathbf{P_8}$-**8** (47 °C), $\mathbf{P_{12}}$-**8** (62 °C), at 0.342 mM). (2) Increasing the number of amino acid residues in the M-PEG "combs" lowered the LCSTs (Figure 2a, serial 1: $\mathbf{P_6}$-**8** (31 °C), $\mathbf{P_6}$-**12** (10 °C); serial 2: $\mathbf{P_8}$-**8** (47 °C), $\mathbf{P_8}$-**12** (26 °C); serial 3: $\mathbf{P_{12}}$-**8** (62 °C), $\mathbf{P_{12}}$-**12** (43 °C), at 0.342 mM). Concentration of the M-PEG "combs" also played a role in the LCSTs, that is, the higher concentration the slightly lower LCSTs (Figure 2a,b). In addition, the LCSTs may be tuned by mixing two M-PEG "combs" (Figure 2c). The LCST of M-PEG "combs" mixture was between the LCSTs of two-component M-PEG "combs" (Figure 2d). It is noteworthy that pure M-PEG "combs" gave much sharper LCSTs than their mixtures, which illustrated the crucial role of structural accuracy for sharp LCSTs and LCSTs fine-tuning. Because regular PEG are mixture of oligomers, replacing the M-PEGs fragments in the M-PEG "combs" with regular PEG fragments would resulted in polydisperse structure, much wider LCSTs, and difficulty in LCSTs fine-tuning. Photos of sequential turbidity changes in the range of 10 to 62 °C further illustrated the LCSTs fine-tuning through accurate structure modification (Figure 2e−j). Interestingly, the limpidity−turbidity transition at the LCSTs was reversible and the turbid solutions of M-PEG "combs" turned into clear solution again when cooling the turbid solutions below their LCSTs. Therefore, a preferred LCST round body temperature for certain biomedical applications would be obtained through these fine-tunings: accurately structural modification, concentration manipulation, and mixing of two M-PEG "combs".

DOI: 10.1021/acs.biomac.8b01693
Biomacromolecules 2019, 20, 1281−1287

To probe the mechanism of limpidity-turbidity transition at LCST, the M-PEG "combs" phase transition was investigated with dynamic light scattering (DLS) and transmission electron microscopy (TEM). DLS showed sharp particle size expansion when heating the M-PEG "combs" from clear solution to turbid solution at LCST (Figure 3a). For example, a particle

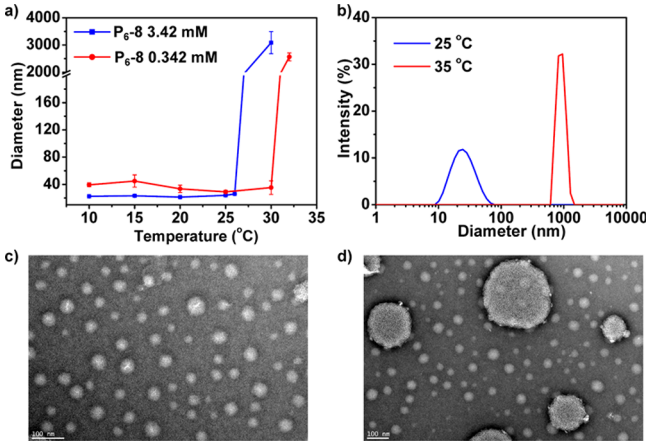

Figure 3. Temperature-dependent DLS of $\mathbf{P_6}$**-8** (a) and its size distributions around LCST (b, 0.342 mM), TEM of $\mathbf{P_6}$**-8** solutions (c: 25 °C, d: 35 °C, 0.342 mM).

size expansion of over 80 times was observed by DLS at the LCST of M-PEG "comb" $\mathbf{P_6}$**-8** (Figure 3b). The sharp particle size expansion of $\mathbf{P_6}$**-8** around LCST was also confirmed by TEM, in which the small nanoparticles of M-PEG "comb" $\mathbf{P_6}$**-8** aggregated into much larger particles above the LCST (Figure 3c,d). It is noteworthy that transformation above LCST is a dynamic process during which small particles keeps aggregating into large particles. So, small particles and large particles were observed in the same TEM image (Figure 3d). Interestingly, TEM showed the formation of long nanotubes with a diameter of about 10 nm in M-PEGs block copolymer $\mathbf{P_8}$**-8′**, which indicated the quite different modes of self-assembly in M-PEG "combs" and M-PEGs block copolymers as a result of the different allocation of hydrophobic groups in the peptidic M-PEGs (see Supporting Information). Therefore, the limpidity−turbid transition at LCST is a result of particle size expansions originated from the peculiar thermosensitive interactions and self-assembly of the M-PEG "combs", during which more M-PEG "combs" aggregated together to form large particles.

To study the thermosensitive behaviors of the M-PEG "combs" on the molecular level, CD and NMR spectra of a model M-PEG "comb", $\mathbf{P_6}$**-8**, were investigated. First, CD spectrum showed that $\mathbf{P_6}$**-8** formed random coils in water at LCST as a result of its highly flexible M-PEGs backbone and the excessive hydrogen bonds between M-PEGs and water (Figure 4a). Second, the hydrophobic interactions of $\mathbf{P_6}$**-8** in water was observed from the ^{19}F chemical shift changes in its solvent-dependent ^{19}F NMR (see Supporting Information). Multiple ^{19}F NMR peaks from 30 pseudosymmetric fluorines in the M-PEG "combs" indicated quite different microenvironment of the trifluoromethyl groups in the self-assembled nanoemulsions. Third, the formation of thermosensitive $\pi-\pi$ stacking among the aromatic groups and hydrophobic interaction among the trifluoromethyl groups were observed from the signal shifting to lower field in the temperature-

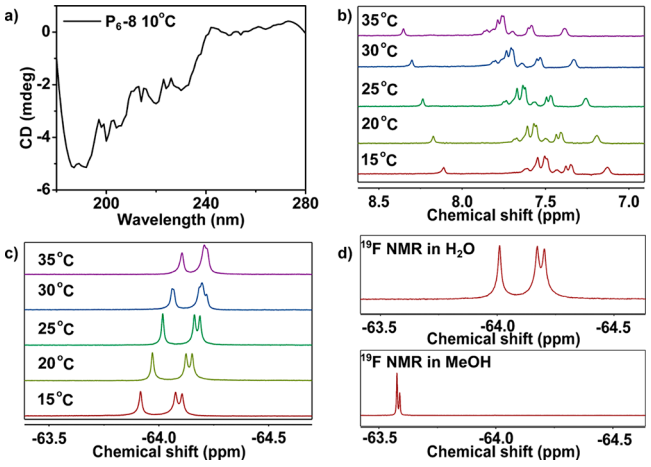

Figure 4. CD spectrum (a) and temperature-dependent (b: ^{1}H NMR, c: ^{19}F NMR) and solvent-dependent (d) NMR of $\mathbf{P_6}$**-8**.

dependent ^{1}H and ^{19}F NMR of $\mathbf{P_6}$**-8** (Figure 4b,c). Enhanced interaction between hydrophobic groups in water was further confirmed by much wider ^{19}F peak distribution of $\mathbf{P_6}$**-8** in water than in methanol (Figure 4d). Based on these observations, thermosensitive interactions between the hydrophobic moieties, including $\pi-\pi$ stacking, hydrophobic interactions and hydrogen bonds, were the driving forces for the phase transition behavior at LCST.

In Vitro ^{19}F MRI and Fluorescent Imaging. The incorporated ^{19}F MRI and fluorescent imaging capability in the M-PEG "combs" were then investigated. M-PEG "comb" $\mathbf{P_{12}}$**-12** with a LCST slightly above body temperature was chosen as a representative M-PEG "comb". First, through the strong ^{19}F signals from its 30 pseudosymmetric fluorines, sensitive ^{19}F MRI was obtained at a low $\mathbf{P_{12}}$**-12** concentration of 0.33 mM with a short scan time of 32 s (Figure 5a). Comparing to fluorescent imaging (sub-μM level), ^{19}F MRI (mM level) is not a sensitive imaging modality.[32,35] $\mathbf{P_{12}}$**-12** with a ^{19}F MRI detectable concentration of 0.33 mM would be regarded as a highly sensitive imaging agent. Relatively short ^{19}F relaxation times were found for $\mathbf{P_{12}}$**-12** (T_1 = 754 ms and

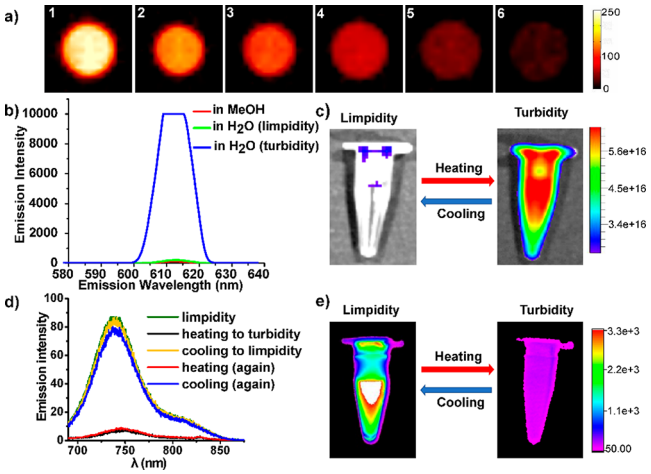

Figure 5. ^{19}F MRI images of $\mathbf{P_{12}}$**-12** (a, $\mathbf{P_{12}}$**-12** concentrations of 1 to 6 are 4.0, 2.7, 2.0, 1.3, 0.67, 0.33 mM, scan time = 32 s, B = 9.4 T), thermoresponsive fluorescent emission curves and images of $\mathbf{P_{12}}$**-12** (b, c, Ex = 305 nm, Em = 613 nm) and BODIPY-loaded $\mathbf{P_{12}}$**-12** nanoemulsion (d, e, Ex = 690 nm, Em = 750 nm).

DOI: 10.1021/acs.biomac.8b01693
Biomacromolecules 2019, 20, 1281−1287

T_2 = 142 ms, 3.42 mM in water, 37 °C), which also contribute to its high ^{19}F MRI sensitivity by shortening the ^{19}F MRI data collection time. As a "hot spot" imaging technique, ^{19}F MRI may conveniently and sensitively track the M-PEG "combs" without ionizing radiation, tissue depth limit, and background signal. Second, through its 2-naphthoyl group, M-PEG "combs" **P_{12}-12** gave thermoresponsive fluorescent images. As a result of thermoresponsive phase transitions at LCST, an over 50 times of fluorescent intensity enhancement at 613 nm was observed when heating **P_{12}-12** solution from limpidity to turbidity (Figure 5b) which exhibited as thermoresponsive "off" and "on" fluorescent images (Figure 5c). Meanwhile, thermoresponsive fluorescent images were also generated from fluorescent dye BODIPY-loaded **P_{12}-12** nanoemulsion. On the contrary, an over 10 times of fluorescent intensity reduction at 750 nm was observed when heating the nanoemulsion from limpidity to turbidity (Figure 5d). The thermoresponsive "on" and "off" fluorescent images (Figure 5e) may be a result of BODIPY aggregation induced fluorescent quench at LCST. It is noteworthy that the fluorescent "on" and "off" process can be repeated many times (Figure 5c).

Biocompatibility and Cytotoxicity. A proof-of-concept study using the thermosensitive M-PEG "combs" as "smart" drug delivery vehicles was carried out. First, biocompatibility of the PEG "combs" was evaluated. Biocompatibility assay on murine fibroblast cells (L929 cells) indicated that the length of M-PEGs fragments in the "combs" played an important role in biocompatibility. M-PEG "combs" **P_{12}-12** and **P_{12}-8** containing relatively long dodecaethylene glycol fragments showed negligible cytotoxicity toward L929 cells while M-PEG "combs" **P_6-8** and **P_8-8** containing short hexaethylene glycol and octaethylene glycol fragments showed dramatic cytotoxicity toward L929 cells, especially at concentrations higher than 0.125 mg/mL (Figure 6a). Then, highly biocompatible M-PEG "comb" **P_{12}-12** was chosen as the drug delivery vehicle and cytotoxicity of drug-loaded **P_{12}-12** was investigated. Drug-loaded M-PEG "combs" nanoemulsion with a diameter of 107.4 nm and a polydispersity index of 0.292 were conveniently obtained by mixing an anticancer drug doxorubicin (DOX) with M-PEG "comb" **P_{12}-12** (Figure 6b). The nanoemulsion released DOX much faster at 40 °C than at 37 °C (Figure 6c), which illustrated the possibility of targeted drug delivery to pathologic sites of higher temperature. The DOX-loaded nanoemulsion exhibited higher antiproliferation efficacy toward hepatocellular carcinoma cells (HepG2 cells) than free DOX at 37 °C, Moreover, the DOX-loaded nanoemulsion exhibited higher antiproliferation efficacy at 40 °C than at 37 °C (Figure 6d, IC_{50} of the nanoemulsion at 37 and 40 °C are 2.7 and 1.3 μg/mL, respectively). Confocal laser scanning microscopy analysis indicated that DOX-loaded **P_{12}-12** nanoemulsion can cross HepG2 cell membrane more efficiently than free DOX (Figure 6e). Therefore, M-PEG "comb" **P_{12}-12** is an effective thermoresponsive drug delivery vehicle for in vitro DOX delivery.

In Vivo Fluorescent Images. Finally, a proof-of-concept image-traceable drug delivery in cells and mice was carried out on BODIPY-loaded **P_{12}-12** nanoemulsion with BODIPY as an imaging-traceable model "drug". Confocal laser scanning microscopy showed that BODIPY-loaded **P_{12}-12** can more effectively delivery the payload, BODIPY, into HepG2 cells, especially into nucleus, than free BODIPY (Figure 7a), which is in consistent with the cytotoxicity results. With a xenograft nude mice model, in vivo fluorescent images showed a long

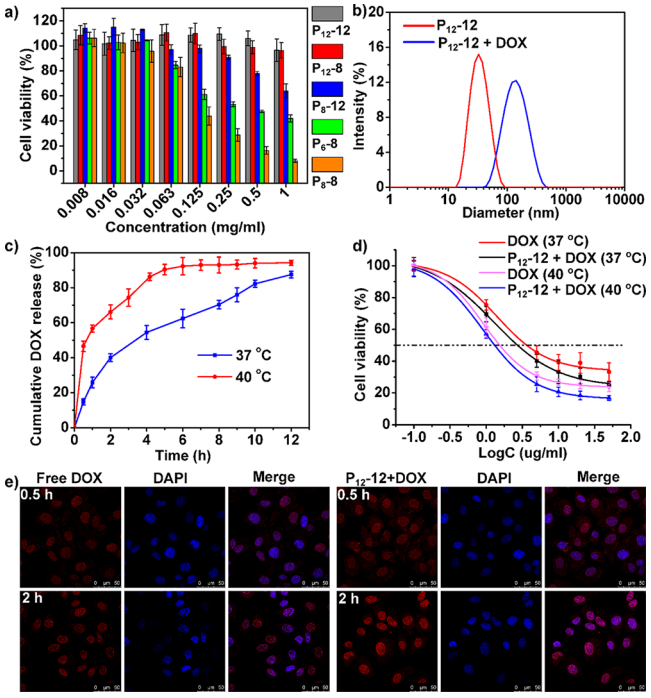

Figure 6. Biocompatibility of the peptides on L929 cells after cultivation for 24 h (a), DLS (b) and DOX release curves of **P_{12}-12** + DOX nanoemulsion (c), antiproliferation efficacy (d), and confocal images (e) of DOX and **P_{12}-12** + DOX nanoemulsion treated HepG2 cells. Values are the means ± s.d. (n = 6 for a, n = 3 for c, d).

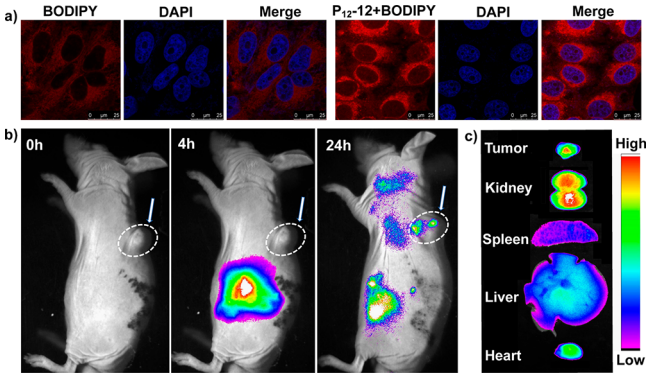

Figure 7. Fluorescent image-guided drug delivery in HepG2 cell after cultivation for 12 h (a), mice (b) and organs after 24 h of intravenous injection (c) with BODIPY-loaded **P_{12}-12** nanoemulsion.

circulating time of the drug delivery system and considerable payload accumulation in tumor (Figure 7b,c). It should be pointed out that, in this case, the **P_{12}-12** dosage of 19.4 μmol/kg is too low to detect **P_{12}-12** in mice with ^{19}F MRI.

CONCLUSION

In summary, we developed thermosensitive and image-traceable M-PEG "combs" as versatile biomaterials. Comparing to thermosensitive PEG block copolymers with polydisperse components, high molecular weight (usually >10 000 Da), and unpredictable LCST, the M-PEG "combs" are featured with accurate and programmable chemical structures, low molecular weights of 3000−6000 Da, sharp and fine-tunable LCSTs, and "hot spot" and "smart" imaging modalities. The accurately structural manipulations of the M-PEG "combs", especially manipulating the size of M-PEGs ω-amino acid and peptide,

DOI: 10.1021/acs.biomac.8b01693
Biomacromolecules 2019, 20, 1281−1287

make LCST and biocompatibility fine-tunable, where M-PEGs act as solubility enhancer, biocompatibility and LCST modulator. It was found that the reversible limpidity−turbidity transition at LCST is a result of thermoresponsive phase transition in self-assembly of the amphiphilic M-PEG "combs", which is accompanied by thermoresponsive "on" and "off" fluorescent imaging from both host, the M-PEG "combs", and guest, loaded cargos, in the micelle system. The multiple pseudosymmetrical fluorines and 2-naphthoyl group in the M-PEG "combs" endow the drug delivery system with "hot spot" and "smart" imaging modalities which facilitate the M-PEG "combs" as "smart" and imaging-traceable biomaterials. The M-PEG "combs" can load and deliver DOX into cells with high efficacy and release DOX in a thermoresponsive fashion. In a proof-of-concept mice study, the M-PEG "combs"-based drug delivery system effectively delivers the payload to tumor in an image-traceable way. Notable, the flexibility of peptide synthesis would provide the M-PEG "combs" with many functions for potential applications, such as targeted delivery, controlled drug release, theranostics, biodegradability, and beyond. On account of their advantages in structural accuracy and diversity, fine-tunable LCST, biocompatibility, drug delivery capability, and versatile multiple imaging modalities, the M-PEG "combs" may find broad applications in biomedicine. Using the peptides as "smart" drug carriers in image-guided cancer therapy on animal models is currently in progress and will be published in due course.

■ ASSOCIATED CONTENT

Supporting Information

The Supporting Information is available free of charge on the ACS Publications website at DOI: 10.1021/acs.biomac.8b01693.

Solvent-dependent ^{19}F NMR, turbidity test, DLS, TEM, synthesis of peptides and drug-loaded micelles, IC_{50} and cytotoxicity assay, cell uptake, in vitro and in vivo imaging, and copies of spectra (PDF).

■ AUTHOR INFORMATION

Corresponding Author

*E-mail: zxjiang@whu.edu.cn.

ORCID

Zhigang Yang: 0000-0002-4857-4850

Xin Zhou: 0000-0002-5580-7907

Zhong-Xing Jiang: 0000-0003-2601-4366

Notes

The authors declare no competing financial interest.

■ ACKNOWLEDGMENTS

We are thankful for financial support from the National Key R&D Program of China (2016YFC1304704), the National Natural Science Foundation of China (21572168, and 81625011), and the Key Research Program of Frontier Sciences, CAS (QYZDY-SSW-SLH018).

■ REFERENCES

(1) Gong, C.; Qi, T.; Wei, X.; Qu, Y.; Wu, Q.; Luo, F.; Qian, Z. Thermosensitive polymeric hydrogels as drug delivery systems. *Curr. Med. Chem.* **2012**, *20*, 79−94.

(2) Mura, S.; Nicolas, J.; Couvreur, P. Stimuli-responsive nanocarriers for drug delivery. *Nat. Mater.* **2013**, *12*, 991−1003.

(3) Torchilin, V. P. Multifunctional, stimuli-sensitive nanoparticulate systems for drug delivery. *Nat. Rev. Drug Discovery* **2014**, *13*, 813−827.

(4) Blanco, E.; Shen, H.; Ferrari, M. Principles of nanoparticle design for overcoming biological barriers to drug delivery. *Nat. Biotechnol.* **2015**, *33*, 941−951.

(5) Biswas, S.; Kumari, P.; Lakhani, P. M.; Ghosh, B. Recent advances in polymeric micelles for anti-cancer drug delivery. *Eur. J. Pharm. Sci.* **2016**, *83*, 184−202.

(6) Li, J.; Mooney, D. J. Designing hydrogels for controlled drug delivery. *Nat. Rev. Mater.* **2016**, *1*, 16071.

(7) Sun, T.; Zhang, Y. S.; Pang, B.; Hyun, D. C.; Yang, M.; Xia, Y. Engineered nanoparticles for drug delivery in cancer therapy. *Angew. Chem., Int. Ed.* **2014**, *53*, 12320−12364.

(8) Wang, Y.; Shim, M. S.; Levinson, N. S.; Sung, H. W.; Xia, Y. Stimuli responsive materials for controlled release of theranostic agents. *Adv. Funct. Mater.* **2014**, *24*, 4206−4220.

(9) Lokerse, W. J.; Kneepkens, E. C.; ten Hagen, T. L.; Eggermont, A. M.; Grull, H.; Koning, G. A. In depth study on thermosensitive liposomes: optimizing formulations for tumor specific therapy and in vitro to in vivo relations. *Biomaterials* **2016**, *82*, 138−150.

(10) Wu, P.; Jia, Y.; Qu, F.; Sun, Y.; Wang, P.; Zhang, K.; Xu, C.; Liu, Q.; Wang, X. Ultrasound-responsive polymeric micelles for sonoporation-assisted site-specific therapeutic action. *ACS Appl. Mater. Interfaces* **2017**, *9*, 25706−25716.

(11) Lokerse, W. J.; Eggermont, A. M.; Grüll, H.; Koning, G. A. Development and evaluation of an isolated limb infusion model for investigation of drug delivery kinetics to solid tumors by thermosensitive liposomes and hyperthermia. *J. Controlled Release* **2018**, *270*, 282−289.

(12) Chen, L.; Ci, T.; Yu, L.; Ding, J. Effects of molecular weight and its distribution of PEG block on micellization and thermogellability of PLGA−PEG−PLGA copolymer aqueous solutions. *Macromolecules* **2015**, *48*, 3662−3671.

(13) Custers, J.; van Nispen, S. F.; Can, A.; de La Rosa, V. R.; Maji, S.; Schubert, U. S.; Keurentjes, J. T.; Hoogenboom, R. Reversible calcium (II) ion binding through an apparent pKa shift of thermosensitive block copolymer micelles. *Angew. Chem., Int. Ed.* **2015**, *54*, 14085−14089.

(14) Bathfield, M.; Reboul, J.; Cacciaguerra, T.; Lacroix-Desmazes, P.; Gérardin, C. Thermosensitive and drug-loaded ordered mesoporous silica: a direct and effective synthesis using PEO-b-PNIPAM block copolymers. *Chem. Mater.* **2016**, *28*, 3374−3384.

(15) Eslahi, N.; Simchi, A.; Mehrjoo, M.; Shokrgozar, M. A.; Bonakdar, S. Hybrid cross-linked hydrogels based on fibrous protein/block copolymers and layered silicate nanoparticles: tunable thermosensitivity, biodegradability and mechanical durability. *RSC Adv.* **2016**, *6*, 62944−62957.

(16) Li, P.; Zhang, Z.; Su, Z.; Wei, G. Thermosensitive polymeric micelles based on the triblock copolymer poly (d, l lactide) b poly (N isopropyl acrylamide) b poly (d, l lactide) for controllable drug delivery. *J. Appl. Polym. Sci.* **2017**, *134*, 45304.

(17) Wu, H.; Liu, G.; Zhang, S.; Shi, J.; Zhang, L.; Chen, Y.; Chen, F.; Chen, H. Biocompatibility, MR imaging and targeted drug delivery of a rattle-type magnetic mesoporous silica nanosphere system conjugated with PEG and cancer-cell-specific ligands. *J. Mater. Chem.* **2011**, *21*, 3037−3045.

(18) Xu, L.; Yang, J.; Xue, B.; Zhang, C.; Shi, L.; Wu, C.; Su, Y.; Jin, X.; Liu, Y.; Zhu, X. Molecular insights for the biological interactions between polyethylene glycol and cells. *Biomaterials* **2017**, *147*, 1−13.

(19) Caddeo, C.; Pucci, L.; Gabriele, M.; Carbone, C.; Fernàndez-Busquets, X.; Valenti, D.; Pons, R.; Vassallo, A.; Fadda, A. M.; Manconi, M. Stability, biocompatibility and antioxidant activity of PEG-modified liposomes containing resveratrol. *Int. J. Pharm.* **2018**, *538*, 40−47.

(20) Zhang, C.; Liu, L. H.; Qiu, W. X.; Zhang, Y. H.; Song, W.; Zhang, L.; Wang, S. B.; Zhang, X. Z. A Transformable chimeric peptide for cell encapsulation to overcome multidrug resistance. *Small* **2018**, *14*, 1703321.

DOI: 10.1021/acs.biomac.8b01693
Biomacromolecules 2019, 20, 1281−1287

(21) Wieczorek, S.; Remmler, D.; Masini, T.; Kochovski, Z.; Hirsch, A. K.; Börner, H. G. Fine-tuning nanocarriers specifically toward cargo: a competitive study on solubilizing related photosensitizers for photodynamic therapy. *Bioconjugate Chem.* **2017**, *28*, 760−767.
(22) Wilke, P.; Börner, H. G. Revealing the impact of poly (ethylene oxide) blocks on enzyme activable coatings from peptide−polymer conjugates. *Eur. Polym. J.* **2015**, *62*, 374−379.
(23) Wieczorek, S.; Dallmann, A.; Kochovski, Z.; Börner, H. G. Advancing drug formulation additives toward precision additives with release mediating peptide interlayer. *J. Am. Chem. Soc.* **2016**, *138*, 9349−9352.
(24) Celasun, S.; Du Prez, F. E.; Börner, H. G. PEGylated precision segments based on sequence defined thiolactone oligomers. *Macromol. Rapid Commun.* **2017**, *38*, 1700688.
(25) Ahmed, S. A.; Tanaka, M. Synthesis of Oligo(ethylene glycol) toward 44-mer. *J. Org. Chem.* **2006**, *71*, 9884−9886.
(26) Maranski, K.; Andreev, Y. G.; Bruce, P. G. Synthesis of poly(ethylene oxide) approaching monodispersity. *Angew. Chem., Int. Ed.* **2014**, *53*, 6411−6413.
(27) Székely, G.; Schaepertoens, M.; Gaffney, P. R. J.; Livingston, A. G. Beyond PEG2000: synthesis and functionalisation of monodisperse PEGylated homostars and clickable bivalent polyethyleneglycols. *Chem. - Eur. J.* **2014**, *20*, 10038−10051.
(28) Zhang, H.; Li, X.; Shi, Q.; Li, Y.; Xia, G.; Chen, L.; Yang, Z.; Jiang, Z.-X. Highly efficient synthesis of monodisperse poly (ethylene glycols) and derivatives through macrocyclization of oligo (ethylene glycols). *Angew. Chem., Int. Ed.* **2015**, *54*, 3763−3767.
(29) Knop, K.; Hoogenboom, R.; Fischer, D.; Schubert, U. S. Poly (ethylene glycol) in drug delivery: pros and cons as well as potential alternatives. *Angew. Chem., Int. Ed.* **2010**, *49*, 6288−6308.
(30) Pelegri-O'Day, E. M.; Lin, E.-W.; Maynard, H. D. Therapeutic protein−polymer conjugates: advancing beyond PEGylation. *J. Am. Chem. Soc.* **2014**, *136*, 14323−14332.
(31) Styslinger, T. J.; Zhang, N.; Bhatt, V. S.; Pettit, N.; Palmer, A. F.; Wang, P. G. Site-selective glycosylation of hemoglobin with variable molecular weight oligosaccharides: potential alternative to PEGylation. *J. Am. Chem. Soc.* **2012**, *134*, 7507−7515.
(32) Bo, S.; Song, C.; Li, Y.; Yu, W.; Chen, S.; Zhou, X.; Yang, Z.; Zheng, X.; Jiang, Z.-X. Design and synthesis of fluorinated amphiphile as ^{19}F MRI/fluorescence dual-imaging agent by tuning the self-assembly. *J. Org. Chem.* **2015**, *80*, 6360−6366.
(33) Wan, Z.; Li, Y.; Bo, S.; Gao, M.; Wang, X.; Zeng, K.; Tao, X.; Li, X.; Yang, Z.; Jiang, Z.-X. Amide bond-containing monodisperse polyethylene glycols beyond 10000 Da. *Org. Biomol. Chem.* **2016**, *14*, 7912−7919.
(34) Yu, Z.; Bo, S.; Wang, H.; Li, Y.; Yang, Z.; Huang, Y.; Jiang, Z.-X. Application of monodisperse PEGs in pharmaceutics: monodisperse polidocanols. *Mol. Pharmaceutics* **2017**, *14*, 3473−3479.
(35) Bo, S.; Yuan, Y.; Chen, Y.; Yang, Z.; Chen, S.; Zhou, X.; Jiang, Z.-X. In vivo drug tracking with ^{19}F MRI at therapeutic dose. *Chem. Commun.* **2018**, *54*, 3875−3878.
(36) Norsten, T. B.; Guiver, M. D.; Murphy, J.; Astill, T.; Navessin, T.; Holdcroft, S.; Frankamp, B. L.; Rotello, V. M.; Ding, J. Highly fluorinated comb-shaped copolymers as proton exchange membranes (PEMs): improving PEM properties through rational design. *Adv. Funct. Mater.* **2006**, *16*, 1814−1822.
(37) Xu, F.; Ping, Y.; Ma, J.; Tang, G.; Yang, W.; Li, J.; Kang, E.; Neoh, K. Comb-shaped copolymers composed of hydroxypropyl cellulose backbones and cationic poly ((2-dimethyl amino) ethyl methacrylate) side chains for gene delivery. *Bioconjugate Chem.* **2009**, *20*, 1449−1458.
(38) Guo, R.; Liu, Y.; Zhang, Y.; Dong, A.; Zhang, J. Surface modification by self-assembled coating with amphiphilic comb-shaped block copolymers: a solution to the trade-off among solubility, adsorption and coating stability. *Macromol. Res.* **2013**, *21*, 1127−1137.
(39) Liu, M.; Leroux, J.-C.; Gauthier, M. A. Conformation-function relationships for the comb-shaped polymer pOEGMA. *Prog. Polym. Sci.* **2015**, *48*, 111−121.
(40) Hofman, A. H.; ten Brinke, G.; Loos, K. Hierarchical structure formation in supramolecular comb-shaped block copolymers. *Polymer* **2016**, *107*, 343−356.
(41) Schmaljohann, D.; Oswald, J.; Jørgensen, B.; Nitschke, M.; Beyerlein, D.; Werner, C. Thermo-responsive PNiPAAm-g-PEG films for controlled cell detachment. *Biomacromolecules* **2003**, *4*, 1733−1739.

DOI: 10.1021/acs.biomac.8b01693
Biomacromolecules 2019, 20, 1281−1287